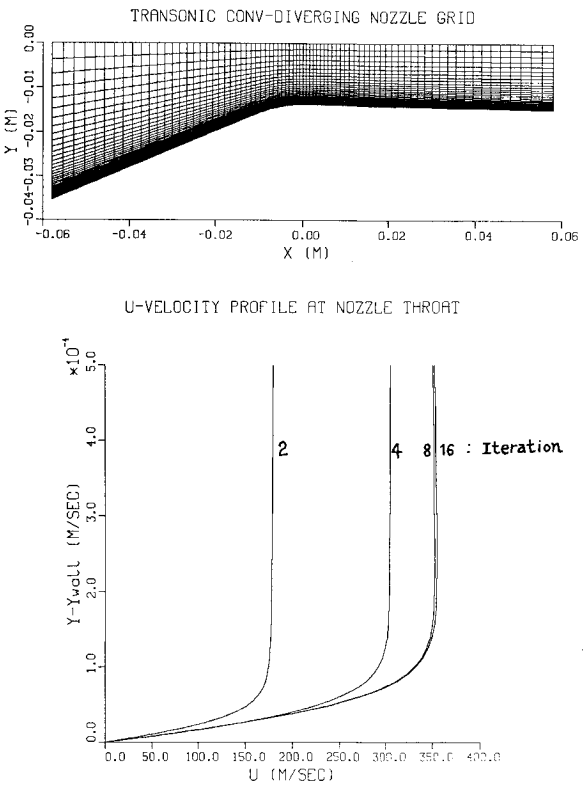

Fig. 1c Convergence of velocity profiles at the nozzle throat: 80×80 mesh.

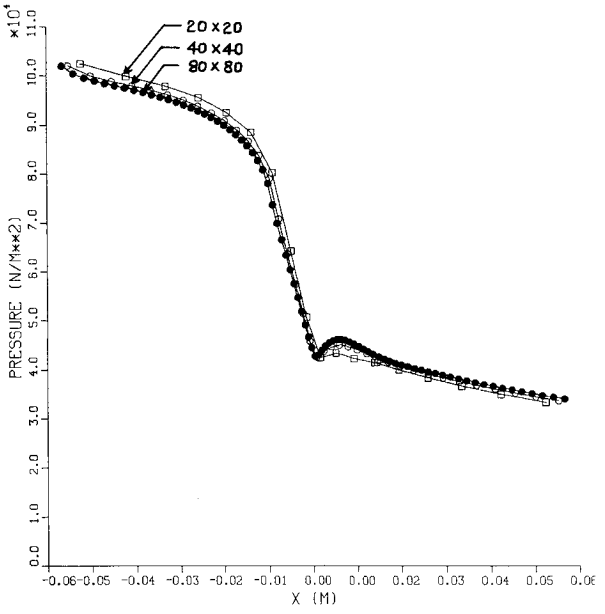

Fig. 2 Pressure along the nozzle wall on 20×20, 40×40, and 80×80 mesh.

in 16 iterations. The numerical results for convergence are shown in Figs. 2 and 3 for the pressure along the nozzle wall and the u component of velocity at the nozzle throat, respectively. They indicate that convergence of the numerical procedure is independent of grid size.

Conclusion

The line Gauss-Seidel relaxation procedures for solving the compressible Navier-Stokes equations show very promising numerical efficiency. The effect of grid size on convergence of the method is tested. The results show that the method is independent of grid size.

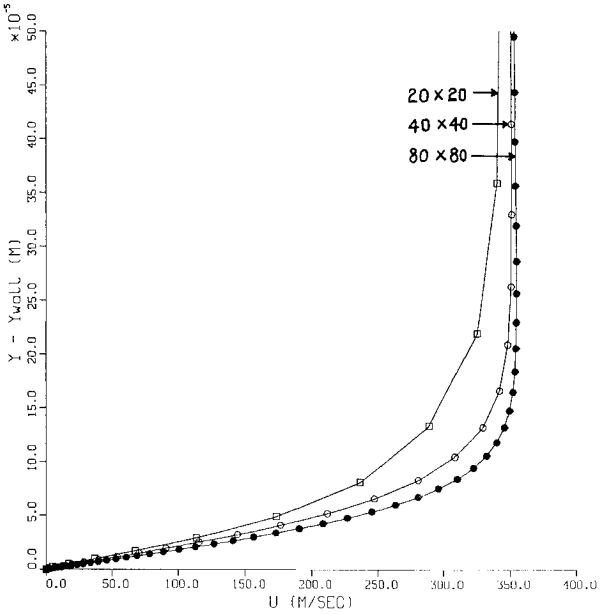

Fig. 3 u component velocity profiles at the nozzle throat on 20×20, 40×40, and 80×80 mesh.

Acknowledgment

The author would like to thank Professor R. W. MacCormack of Stanford University and Applied Computational Aerodynamics Branch at NASA Ames Research Center for help and encouragement.

References

[1]MacCormack, R. W., "Current Status of Numerical Solutions of the Navier-Stokes Equations," AIAA Paper 85-0032, Jan. 1985.

[2]Chakravarthy, S. R., "Relaxation Methods for Unfactored Implicit Upwind Schemes," AIAA Paper 84-0165, Jan. 1984.

[3]Holst, T. L., "Numerical Computation of Transonic Flow Governed by the Full-Potential Equation," Paper presented at Lecture Series, von Kármán Institute, Belgium, 1983.

Spacing of Streamwise Vortices on Concave Walls

Jerry D. Swearingen* and Ron F. Blackwelder†
University of Southern California
Los Angeles, California

Introduction

THE stability of streamwise vortices generated on a concave wall by the Görtler mechanism is governed by the parameter

$$G\ddot{o}_\Theta \equiv (U_\infty \Theta/\nu)\ [\Theta/R]^{1/2}$$

Presented as Paper 83-0380 at the AIAA 21st Aerospace Sciences Meeting, Reno, NV, Jan. 10-13, 1983; received Jan. 15, 1986.

*Research Associate, Department of Aerospace Engineering. Member AIAA.

†Professor, Department of Aerospace Engineering. Member AIAA.

where Θ is the momentum thickness and R is the radius of curvature. Hammerlin[1] and Smith[2] have shown that for $G\ddot{o}_\Theta > 0.3$, streamwise vortices are unstable and grow in the downstream direction. According to linearized theory, the streamwise vortices can assume any spanwise disturbance wave number within a broad range available for amplification. The existing experimental data tends to show, however, that some preferred wave number disturbance is selected initially from those unstable ones and is amplified with increasing $G\ddot{o}_\Theta$ while following lines of constant

$$\Lambda \equiv (U_\infty R/\nu)\,[\lambda/R]^{3/2}$$

This gives rise to a number of questions; in particular, what factors affect the initial selection of a preferred disturbance, and can the selection be controlled in some way? The following investigation was undertaken to explore these particular points.

Previous experimental evidence on spanwise wavelength selection for a boundary layer growing on a concave wall consists primarily of the work of Tani,[3] Tani and Sakagami,[4] and Bippes.[5] Tani found the spanwise wave number to be independent of the streamwise location, freestream velocity, and the spanwise test section dimension. This led to his conjecture that the observed wave number is an inherent feature of the test configuration, provided it is in the unstable regime. Bippes found the spanwise spacing of streamwise vortices to be dependent on the nature of the disturbance field, and that the most amplified wavelength predicted by the theory could be observed experimentally if the disturbances in the freestream were made as isotropic as possible. The theoretical work of Floryan and Saric[6] showed that the selection mechanism is easily affected by deviations from ideal flow conditions. For example, inhomogeneities in the mean flowfield, such as residual streamwise vorticity, may result in spanwise wavelengths different from the most amplified ones.

Evidence also exists that flat-plate boundary layers have a preferential selection mechanism. A number of experimentalists have noted spanwise irregularities in mean flow properties within the boundary layer that can best be described by the presence of streamwise vortices. An example of this is the study of Anders and Blackwelder[7] who found spanwise variations associated with the vorticity to be independent of screen properties, freestream velocity, and leading-edge geometry. Using a perturbation analysis, Crow[8] found that a laminar boundary layer is extremely sensitive to small spanwise velocity variations, which can result in a boundary layer having a "wavy" character in the spanwise direction. The overall conclusion to be drawn from the previous work is that inhomogeneities in the conditions upstream of the boundary layer can lead to preferential selection of a spanwise wave number associated with the appearance of streamwise vortices.

Apparatus and Tests

The experiments were performed in a low-speed wind tunnel specially designed so that the laminar boundary layer generated on the concave working surface would become unstable to the Görtler instability earlier than to the Tollmien-Schlichting instability. The tunnel is an open return type in which a variable speed 10,000 cfm axial blower produces the required velocity in the test section. A small angle diffuser (½angle< 3 deg) connects the blower with a 122 × 122 cm settling chamber. The upstream portion of the settling chamber consists of five removable frames, each having interior dimensions of 122 × 122 × 15 cm, constructed to provide smooth interior walls. The upstream frame contains a honeycomb section with cells 1 cm in diameter and 10 cm long. Four fine mesh screens are attached to the remaining frames. Downstream, a fifth-order polynomial contraction reduces the flow area to 122 × 18 cm at its exit. The sidewall boundary layers at the exit of the contraction are removed by auxiliary blowers through a 1.5 cm suction slot concentric with the test section leading edge. The suction slot is perpendicular to the mean flow and reduces the cross-sectional area to 119 × 15 cm at the beginning of the test section. This provides a distinct origin for the boundary layer at the leading edge of the curved plate, which is 240 cm long and has a 320 cm radius of curvature. The concave working surface has a rounded leading edge coinciding with the origin of the streamwise coordinate x.

Measurements of the streamwise static pressure distribution show C_p deviation along the test section center line to be less than 5% for freestream velocities in the range 2.5–10 m/s. Spanwise traverses of the freestream velocity show deviation of less than 0.5% across the test section exclusive of top and bottom wall boundary layers. Freestream turbulence level in the working section was measured to be less than 0.07% U_∞ for all test velocities.

During these experiments, the freestream velocity varied in the range of 2–12 m/s yielding $3 < G\ddot{o}_\Theta < 10$, and $10^5 < Re_x < 5 \times 10^5$ for the streamwise locations explored. Since the system of vortices produced by the Görtler instability has no temporal variation of the streamwise velocity, the flowfield was primarily studied by continuously traversing a single hot-wire probe over a large spanwise distance. The probe was mounted on a streamlined sled riding on the working surface in order to maintain a constant y/δ_L position at all spanwise locations and was used at a number of streamwise locations.

Results and Discussion

Initial results show that a system of streamwise vortices fixed in space is found on the test wall as evidenced by a periodic variation of the streamwise component of mean velocity as in Fig. 1a. The observed spanwise wavelength is roughly 2.3 cm independent of downstream location and corresponds to $\Lambda \sim 670$. This information is in good agreement with stability analyses of the Görtler problem and the experimental results of Tani[3] and Tani and Sakagami.[4]

Among the factors considered potentially important in the selection of a preferred spanwise wavelength, those affecting

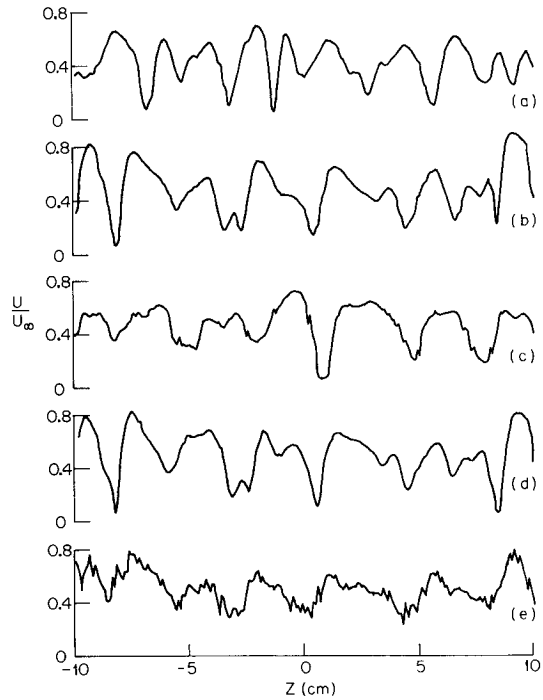

Fig. 1 Spanwise distributions of mean streamwise velocity for various freestream conditions at fixed $y/\delta_L = 0.25$ with $x = 82.5$ cm and $U_\infty = 5$m/s. a) 24 mesh, 72% open screens, b) 40 mesh, 72% open screens, c) 40 mesh screens but with the last screen having 44% open area, d) three 40 mesh screens with blank insertion in last screen position, e) 40 mesh screens with honeycomb removed.

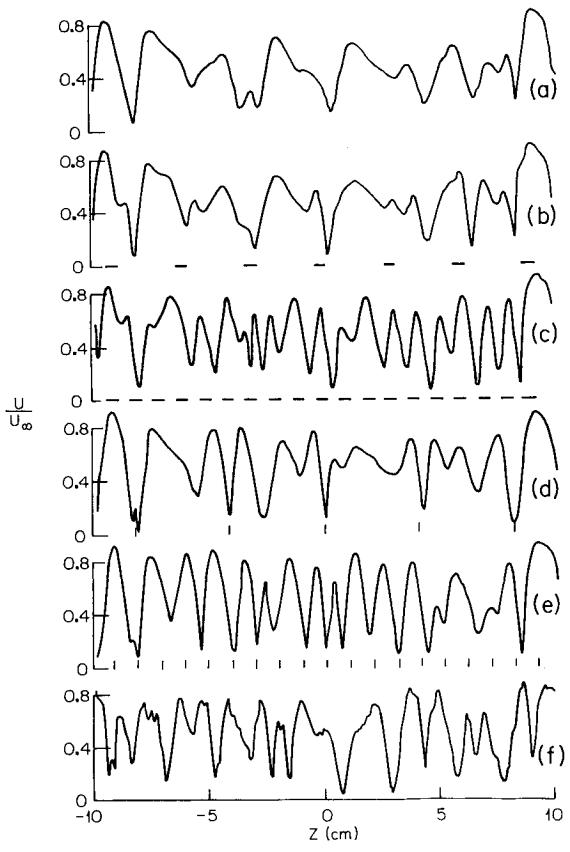

Fig. 2 Spanwise distributions of mean streamwise velocity at $U_\infty = 5$ m/s, $x = 82.5$ cm, and $y/\delta_L = 0.25$ for various perturbation schemes (four 40 mesh, 72% open stilling section screens in place). a) no perturbation used, b) cellophane tape spacers 3.0 cm apart (the locations of the tape spacers are indicated by the horizontal bars), c) tape spacers 1.0 cm apart, d) 0.01 cm diam cylinders upstream of leading edge at $Re_d \sim 7.0$ with spanwise spacing of 4.0 cm (tick marks indicate the cylinder positions), e) cylinders 1.0 cm apart, f) 10 mesh, 56% open screen in front of leading edge at $Re_d \sim 60$.

the freestream properties were investigated most thoroughly. A reference condition of $U_\infty = 5$m/s, $x = 82.5$ cm, and $y/\delta_L = 0.25$ was chosen for comparison of spanwise traverses to detect the periodic variation of the streamwise velocity component where δ_L is the nominal Blasius boundary layer thickness. Figures 1a and 1b show results taken with two different sets of settling chamber screens having 24 and 40 mesh sizes but with the same open area of 72%. It is obvious that the details of the peak and valley structure change substantially between the two; however, it is difficult to discern a significant difference in the spanwise wavelength. This typically occurred every time the last screen was changed, i.e., the pattern changed notably but the average wavelength remained constant. Figure 1c shows a traverse with the 40 mesh screens but with the downstream screen replaced with one having 44% open area. Again, the spanwise wavelength remains essentially unchanged. The effects of several other changes are also noted in the figure. Removing the third screen, moving the last 40 mesh screen upstream, and inserting an empty frame in the last position increased the effective damping length for the residual turbulence by 300 mesh lengths. Figure 1d indicates that there is no difference in the observed spanwise structure. Similarly, Fig. 1e indicates that removal of the honeycomb section upstream of the screens did not alter the spanwise wavelength although a substantial increase in freestream turbulence level was noted.

The effects of freestream velocity and test section transverse dimension on the spanwise wavelength also were tested. Although not shown, a change in velocity over the range 2.5–10 m/s appeared not to change the spanwise wavelength substantially. Likewise, by inserting false walls, a reduction by a factor of 2 in the spanwise test section dimension did not alter the wavelength or spanwise pattern.

Different perturbation schemes were investigated to determine their effect on the selection of a preferred spanwise wavelength. Figure 2 shows the results of these various schemes using a reference condition of $U_\infty = 5$ m/s, $x = 82.5$ cm, and $y/\delta_L = 0.25$. For comparison, Fig. 2a gives a traverse using no perturbations. Figures 2b and 2c utilize the technique of Klebanoff et al.[9] of placing cellophane tape strips on the solid surface to position the boundary layer's spanwise variation. Strips of 0.008 cm thick tape 0.5 cm wide by 1.9 cm long were installed on the concave plate surface 1.0 cm downstream of the leading edge for various spanwise spacings. This x location yielded a Görtler parameter of approximately 0.25, which is near the minimum value needed for instability. With the tapes spaced 3.0 cm apart, i.e., greater than the measured natural wavelength, Fig. 2b shows very little change in the observed pattern. Note, however, that a small amount of additional structure appears to be added. In contrast, a spanwise perturbation having a wavelength less than the natural wavelength affects the spanwise structure substantially. In Fig. 2c, the measured wavelength is approximately 1.0 cm, which is the same as the tape spacing. Disturbances in the upstream flowfield were obtained by placing 0.01 cm diameter cylinders at selectable spanwise locations upstream of the test plate in the contraction. The Reynolds number based on cylinder diameter was ~7.0. This novel technique produces streamwise vortices when the vortical wakes of the cylinders intersect the leading edge and are stretched by the boundary layer. A cylinder spacing of 4.0 cm, i.e., greater than the natural wavelength, does not substantially alter the overall spanwise structure as seen in Fig. 2d. However, the additional streamwise vorticity imposed by the cylinder wakes is clearly visible as they form narrow regions of low-speed fluid superimposed on the naturally occurring structure. On the other hand, a spanwise spacing of 1.0 cm gives a fairly uniform periodic variation in Fig. 2e approximately corresponding to the cylinder spacing.

One additional means of controlling the spanwise wavelength was investigated. Earlier results of Bippes[5] showed that a disturbance wavelength close to the most amplified one could be forced in the boundary layer using screens placed upstream of the plate's leading edge to create an isotropic disturbance field. Schubauer et al.[10] showed that screen disturbances are damped below a critical Reynolds number depending on the screen solidity ratio. This effect was studied by placing a 10 mesh, 56% open area screen in the contraction upstream of the test plate at two locations, one above and one below the calculated $Re_{CR} = 50$. Figure 2f shows the spanwise pattern found for $Re > Re_{CR}$. The measured spanwise wavelength approximately corresponds to the value predicted by linear theory as the most amplified disturbance. Similar results for the subcritical case suggest that the screen's Reynolds number is not an important parameter. The screen results are in good qualitative agreement with the findings of Bippes.

Conclusion

Various conditions affecting the selection of a preferred spanwise wavelength in the establishment of streamwise vortices by the Görtler instability mechanism on a concave wall were studied. The principal results are: 1) A system of streamwise vortices fixed in space evolves on the test wall roughly independent of Reynolds and Görtler numbers. 2) The spanwise wavelength appears to be independent of screen geometry, test section spanwise dimension, effective turbulence damping length after the last stilling screen, or the presence of honeycomb in the stilling chamber. The measured spanwise *pattern* does, however, depend strongly on the last settling chamber screen. 3) Perturbations of the freestream properties can affect the observed spanwise wavelength to a certain ex-

tent. The boundary layer appears to be most responsive to disturbances close to the most amplified ones.

Acknowledgment

The authors would like to thank the Air Force Office of Scientific Research for their support of this work through Contract F49620-78-C-0060.

References

[1]Hämmerlin, G., "Über das Eigenwertproblem der dreidimensionalen Instabilität laminarer Grenzschichten an konkaven Wänden," *Journal Rational Mechanics and Analysis,* Vol. 4, No. 2, 1955, pp. 279-321.

[2]Smith, A.M.O., "On the Growth of Taylor-Görtler Vortices Along Highly Concave Walls," *Quarterly of Applied Mathematics,* Vol. 13, No. 3, 1955, pp 233-262.

[3]Tani, I., "Production of Longitudinal Vortices in the Boundary Layer Along a Concave Wall," *Journal of Geophysical Research,* Vol. 67, No. 8, 1962, pp. 3075-3080.

[4]Tani, I. and Sakagami, J., "Boundary-Layer Instability at Subsonic Speeds," *Proceedings of Third Congress of International Council of Aerospace Sciences,* Spartan, Washington, DC 1964, pp. 391-403.

[5]Bippes, H., "Experimentelle Untersuchung de laminar-turbulenten Umschlags an einer parallel angeströmten konkaven Wand," Mathematisch-naturwissenschaftliche klasse, Heidelberger Akademie der Wissenschaften, Sitzungsberichte, No. 3, 1972, pp. 103-180, also NASA-TM-75243, March 1978.

[6]Floryan, J. and Saric, W., "Wavelength Selection and Growth of Görtler Vortices," AIAA Paper 80-1376, July 1980.

[7]Anders, J. and Blackwelder, R., "Longitudinal Vortices in a Transitioning Boundary Layer," *Laminar-Turbulent Transition, Proceedings of IUTAM Symposium,* edited by R. Eppler and H. Fassel, Springer-Verlag, Berlin, 1980, pp. 110-119.

[8]Crow, S., "The Spanwise Perturbation of Two-Dimensional Boundary Layers," *Journal of Fluid Mechanics,* Vol. 24, Pt. 1, 1966, pp. 153-164.

[9]Klebanoff, P., Tidstrom, K., and Sargent, L., "Three-Dimensional Nature of Boundary-Layer Instability," *Journal of Fluid Mechanics,* Vol. 12, Pt. 1, 1962, pp. 1-34.

[10]Schubauer, G., Spangenberg, W., and Klebanoff, P., "Aerodynamic Characteristics of Damping Screens," NACA TN 2001, 1950.

Formulas for Venting or Charging Gas from a Single Volume

H. T. Yang*
Hughes Aircraft Company, Canoga Park, California

Nomenclature

$a = \left[\frac{2}{k-1}\left(\frac{k+1}{2}\right)^{\frac{k+1}{k-1}}\right]^{1/2}$

A_T = throat area
C_D = discharge coefficient

$C_1 = \left[\frac{k}{R}\left(\frac{2}{k+1}\right)^{(k+1)/(k-1)}\right]^{1/2}$

k = ratio of specific heats
P = tank pressure
P_f = final tank pressure
P_i = initial tank pressure
P_1 = pressure upstream of nozzle
P_2 = pressure downstream of nozzle
R = gas constant
T_f = final tank temperature
T_i = initial tank temperature
T_1 = temperature upstream of nozzle
t = time
V = tank volume

Received Aug. 26, 1985; revision received Dec. 18, 1985.

*Professor of Aerospace Engineering, University of Southern California, Los Angeles.

Introduction

In working on problem 4.28 in Ref. 1 and later on the nitrogen leakage from an inertial sensor assembly (ISA) and the helium flow in a pneumatic actuator system (PAS), the author developed formulas for the pressure in a venting gas tank as a function of time. The formulas are simple for choked flow, but rather complicated for the unchoked case. However, it is stated in Ref. 2 that "for subcritical (unchoked) flow the equations cannot be solved as easily but can be evaluated by graphical integration." The purpose of this Note is to present analytical expressions for the integrals appearing in Table 3.10.5a of Ref. 2, which was adapted from Ref. 3.

Integrals in Time-Pressure Equations

Based on the energy balance of the isentropic charging a perfect gas into a given volume, the time required for critical flow as given in Ref. 2 (based on Ref. 3) is

$$t_{cr} = \frac{V}{kRC_1C_DA_T\sqrt{T_1}}\left(\frac{P_f}{P_1} - \frac{P_i}{P_1}\right) \tag{1}$$

at

$$0 \le \frac{P}{P_1} \le \left(\frac{2}{k+1}\right)^{k/(k-1)}$$

and for subcritical flow is

$$t_{scr} = \frac{V}{kRC_1C_DA_T\sqrt{T_1}}\frac{1}{a}\int_{P_i/P_1}^{P_f/P_1}\left[\left(\frac{P}{P_1}\right)^{2/k} - \left(\frac{P}{P_1}\right)^{(k+1)/k}\right]^{-1/2} d\left(\frac{P}{P_1}\right) \tag{2}$$

at

$$(2/k+1)^{k/(k-1)} \le P/P_1 \le 1$$

The corresponding times for isothermal charging are

$$t_{cr} = \frac{V\sqrt{T_1}}{C_1C_DA_TRT_i}\left(\frac{P_f}{P_1} - \frac{P_i}{P_1}\right) \tag{3}$$

$$t_{scr} = \frac{V\sqrt{T_1}}{C_1C_DA_TRT_i}\frac{1}{a}\int_{P_i/P_1}^{P_f/P_1}\left[\left(\frac{P}{P_1}\right)^{2/k} - \left(\frac{P}{P_1}\right)^{(k+1)/k}\right]^{-1/2} d\left(\frac{P}{P_1}\right) \tag{4}$$

To carry out the integration in Eqs. (3) and (4), we let

$$\chi = (P/P_1)^{-(k-1)/k}$$

the integral simplifies to

$$I_c = -\frac{k}{k-1}\int_{\chi_i}^{\chi_f}\frac{d\chi}{\chi^{3/2}\sqrt{\chi-1}}$$